

# Improved fracture toughness and fatigue life of carbon fiber reinforced epoxy composite due to incorporation of rubber nanoparticles

Nguyen Tien Phong · Mohamed H. Gabr ·  
Le Hoai Anh · Vu Minh Duc · Andrea Betti ·  
Kazuya Okubo · Bui Chuong · Toru Fujii

Received: 1 January 2013 / Accepted: 23 April 2013 / Published online: 7 May 2013  
© Springer Science+Business Media New York 2013

**Abstract** In this study, core–shell rubber (CSR) nanoparticles with approximate particle size of 35 nm were used as a modifier for the epoxy polymer. The effects of various CSR contents in the epoxy matrix on mode I interlaminar fracture toughness, tensile strength, and fatigue life of the carbon fabric reinforced epoxy (CF/EP) composites were investigated. The experimental results showed that the mode I interlaminar fracture toughness at crack initiation and propagation significantly improved by 71.21 and 58.47 %, respectively, when 8.0 wt% CSR was dispersed in the epoxy matrix. The fatigue life of the modified CF/EP composites at all of CSR contents dramatically increased 75–100 times longer than that of the unmodified CF/EP composites at high cycle fatigue while tensile strength slightly increased by about 10 %. Field emission scanning electron microscopy (FESEM)

observations of the fracture surfaces were conducted to explain failure mechanisms of CSR addition to the CF/EP composites. The evidences of the rubber nanoparticle debonding, plastic void growth, and microshear banding were credited for delaying the onset of matrix crack, and reducing the crack growth rate, as a result, attributed to increase in the mechanical properties of the CF/EP composites.

## Introduction

Carbon fiber reinforced epoxy (CF/EP) composites, because of their high strength, light weight, and versatility, are being considered for use in the design of new advanced aircraft structural component [1–4]. Compared to metallic materials, the CF/EP composite possesses variety of advantageous properties, such as high strength to weight ratio, excellent corrosion resistance, and favorable fatigue tolerance. However, strength properties of the CF/EP composites are sensitive to failure modes, such as transverse cracking, longitudinal cracking, and delamination between adjacent layers due to intrinsic brittleness of epoxy matrix [5, 6].

The recent studies showed that the possibility of the most of failure modes of the fiber reinforced plastics (FRP) composites could be step by step controlled. Their mechanical performances would be dramatically enhanced by incorporating a small amount of nanoscale materials to the epoxy matrix [7, 8]. Takagaki et al. [9] found that with an addition of 0.3 wt% MFC to epoxy matrix, the fatigue life of carbon fabric composites significantly increased by 2,000 %. Davis et al. [3] reported that the tensile strength, stiffness, and tension–tension fatigue appreciably increased due to an addition of a little content of amine-

---

N. T. Phong (✉) · M. H. Gabr · A. Betti · K. Okubo · T. Fujii  
Department of Mechanical Engineering and Systems, Doshisha  
University, Kyotonabe, Kyoto 610-0394, Japan  
e-mail: phongnt42@yahoo.com;  
phongntmatescience@gmail.com

N. T. Phong · V. M. Duc · B. Chuong  
Polymer Center, Hanoi University of Science and Technology,  
No 1, Dai Co Viet, Hanoi, Vietnam

N. T. Phong · L. H. Anh  
Institute of Chemical and Biological Engineering, 80 Tran Quoc  
Hoan, Cau Giay, Hanoi, Vietnam

M. H. Gabr  
Department of Mechanical Engineering, Sohag University,  
Sohag, Egypt

A. Betti  
Department of Structural Engineering, Politecnico di Milan,  
Milan, Italy

functionalized single wall carbon nanotubes (a-SWCNTs) for the CF/EP composites. Li et al. [10] deposited electrospun nano polysulfone fibers, with 230 nm in diameter, directly onto carbon fiber/epoxy prepregs to toughen the composite. They revealed that the mode I interlaminar fracture toughness of the composite at 5 wt% content was 280 % higher than that of the unmodified composite. Hsieh et al. [11] showed that the fracture toughness of the bulk epoxy polymer was increased from 77 to 212 J/m<sup>2</sup> by the presence of 20 wt% silica nanoparticles, and significant increased from 439 to 1316 J/m<sup>2</sup> by combination of 10 wt% silica nanoparticles and 9 wt% rubber microparticles for the interlaminar fracture toughness of the CF/EP composites. Manjunatha et al. [12] stated that the fatigue life of neat epoxy and the glass fiber reinforced epoxy composite (GFRP) improved about three to four times with the addition of 10 wt% silica nanoparticles. Lars Boger et al. [13] showed that the addition of nanoparticles lead to increase in interfibre fracture strength of up to 16 %. The high cycle fatigue life was increased by several orders of magnitude in number of load cycles.

Based on the recent outcomes, nanoparticles have attracted much attention as good reinforcement candidates to toughen epoxy resin and FRP composites. Such nanoparticle modified epoxy and FRP composites have been shown to not only increase the toughness of the epoxy, and mechanical properties of the composites but also due to the very small size of the particles, not to lead to a significant increase in the viscosity, modulus, and glass transition temperature ( $T_g$ ) [14]. However, detailed studies on mode I interlaminar fracture toughness and fatigue behaviors of nanoparticle toughened CF/EP composites have been limited. It is clear that fracture toughness and fatigue behavior of the CF/EP composite with incorporating nanoparticles is still an open problem. Hence, the main objective of the present study is to investigate the effect of CSR-modified epoxy on fracture resistance and fatigue life of the CF/EP composites. The failure mechanisms of CSR addition in the CF/EP composites have been identified and discussed.

## Experimental details

### Materials

Core-shell rubber (CSR) nanoparticles (XER-31) have a crosslinked acrylonitrile butadiene rubber core, and covered with a compatibilizer copolymer shell for epoxy polymer were supplied by JCR Inc. Company, Japan. Particle size of CSR is about 35 nm in diameter. Plain woven carbon cloth (Pyrofil TR3110 M: Mitsubishi Rayon Co., Ltd.) was used as reinforcement, is tensile strength of

which is 3 GPa, Young's modulus of 240 GPa, and density of  $1.8 \times 10^{-3}$  g/mm<sup>3</sup>. Epoxy resin and modified aliphatic polyamine (Japan Epoxy Resins Co., Ltd) were respectively, used as matrix and curing agent.

### Sample preparation

CSR was dispersed with methyl ethyl ketone (MEK) at 80 °C for 24 h using a magnetic stirrer. After that they were homogenized by a homogenizer for 30 min, and then sonicated for 45 min by an ultrasonic process to obtain CSR suspensions with the smallest possible particle size. CSR with various contents (0.0, 3.0, 5.0, and 8.0 wt%) were prepared to examine the effect of the addition of CSR on the mechanical properties of epoxy matrix and the CF/EP composites. The desired amount of epoxy was added into the CSR suspensions, and mixed for 30 min by a homogenizer, and then sonicated for 45 min. The obtained CSR/epoxy mixtures were put into an electric oven for 3 days at 90 °C to remove the MEK. The calculated amount of curing agent was added, and then degassed in a vacuum chamber for 15 min resulting in the CSR/epoxy mixtures. After that the mixture was hand lay-upped with plain woven carbon fiber, and cured at 80 °C for 1 h and 150 °C for 3 h for manufacturing the CF/EP composites. The carbon fiber volume fraction was  $50 \pm 2$  %.

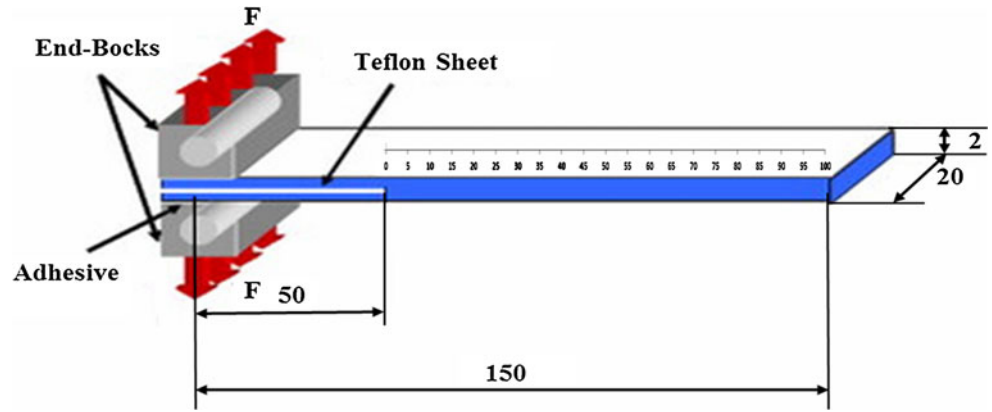
### Tensile test

The tensile properties of the samples were measured using a shimadzu autograph universal testing machine. The specimen gage length was 100 mm and the testing speed was set to 1 mm/min. The approximate dimension of the specimen was  $200 \times 25 \times 2$  mm<sup>3</sup> according to ASTM D3039-08 [15]. Aluminum or glass fiber reinforced plastic (GFRP)/epoxy tabs with a thickness of 2 mm were attached at both ends of the specimen by an adhesive.

### Mode-I interlaminar fracture toughness test

The mode I double cantilever beam (DCB) tests were carried out according to ASTM D5528-01 [16]. The recommended specimen size is at least 150-mm long and 20-mm wide with an initial crack length (i.e., the length of the insert from the line) of 50 mm. Hinges of the same width as the specimen were attached to allow load application. Load and displacement were then related to delamination length as measured with a ruler on the specimen edge (see Fig. 1). The mode I interlaminar fracture toughness  $G_{IC}$  and  $G_{IP}$  for each CSR contents was calculated using the modified compliance calibration (MCC) method. The MCC methods were calculated from Eqs. 1 and 2.

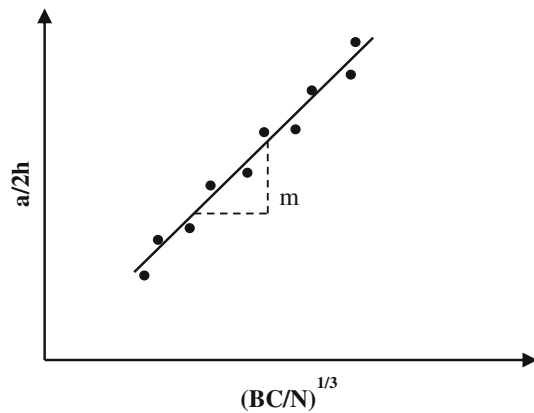
**Fig. 1** Geometry of DCB specimen (all dimensions in mm)



$$G_{IC} = \frac{3m}{2(2h)} \left(\frac{P_c}{B}\right)^2 \left(\frac{BC}{N}\right)^{2/3} F \tag{1}$$

$$G_{IP} = \frac{3m}{2(2h)} \left(\frac{P_p}{B}\right)^2 \left(\frac{BC}{N}\right)^{2/3} F \tag{2}$$

where  $G_{IC}$  is the fracture toughness at initial crack stage,  $G_{IP}$  is the fracture toughness at propagation stage,  $P_p$  is the applied load,  $C$  is the compliance corresponding to each crack length,  $a$  is the crack length,  $P_c$  is the initial maximum load,  $B$  is the specimen width,  $2h$  is the specimen thickness in equation,  $N$  is the end-block correction factor, and  $F$  is the large displacement correction factor,  $m$  is the slope of a plot of  $(BC/N)^{1/3}$  versus  $(a/2h)$ .



Determination of  $m$  using modified compliance calibration (MCC) method.

**Tension–tension fatigue test**

Tension–tension fatigue tests were conducted at the stress-ratio ( $R = +0.1$ ) and a frequency ( $f = 5$  Hz) according to ASTM D3479 [17] on the ServoPulser 50KN equipment. The internal damage was observed from the side of the specimen using an optical microscopy (Keyence VH-Z450).

**Scanning electron microscopy observation**

The fracture surfaces of the testing specimens were observed using field emission scanning electron microscopy (FESEM-JSM-7001FD equipment). Before FESEM observation, all samples were coated with a thin layer of gold to avoid electrical charging.

**Results and discussion**

**Mode-I interlaminar fracture toughness test**

Typical load–displacement curves obtained from double cantilever beam (DCB) tests of the CF/EP composites were shown in Fig. 2. It was seen that there are characteristic stick-slips in all specimens. This can be due to the variations in local material properties, such as resin rich, fiber-rich regions along the longitudinal direction, misalignment of the fibers, voids, and the fracture of bridged fibers or fibers bundles [18]. Moreover, the modified composites performed longer maximum displacements at complete fracture. It was suggested that the crack growth of the modified composites propagated more stable and gradual than that of the unmodified composites.

The delamination resistance curves (R-curves) were drawn between crack length and the corresponding fracture toughness as shown in Fig. 3. The  $G_{IC}$  value corresponding to first crack initiation is determined from the load point at which the initiation of delamination was microscopically observed on the specimen edge. Both delamination initiation and delamination propagation mode-I fracture toughness values were listed in Table 1. The delamination initiation ( $G_{IC}$ ) values were reported throughout this investigation corresponding to first peak load in load-crack opening displacement curves, while the delamination propagation ( $G_{IP}$ ) values were taken from the plateau region of the R-curves [19, 20].

**Fig. 2** Typical load–displacement curves of the CF/EP composites with various CSR contents

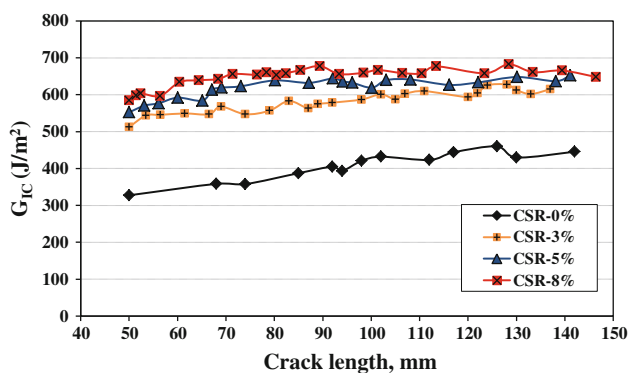
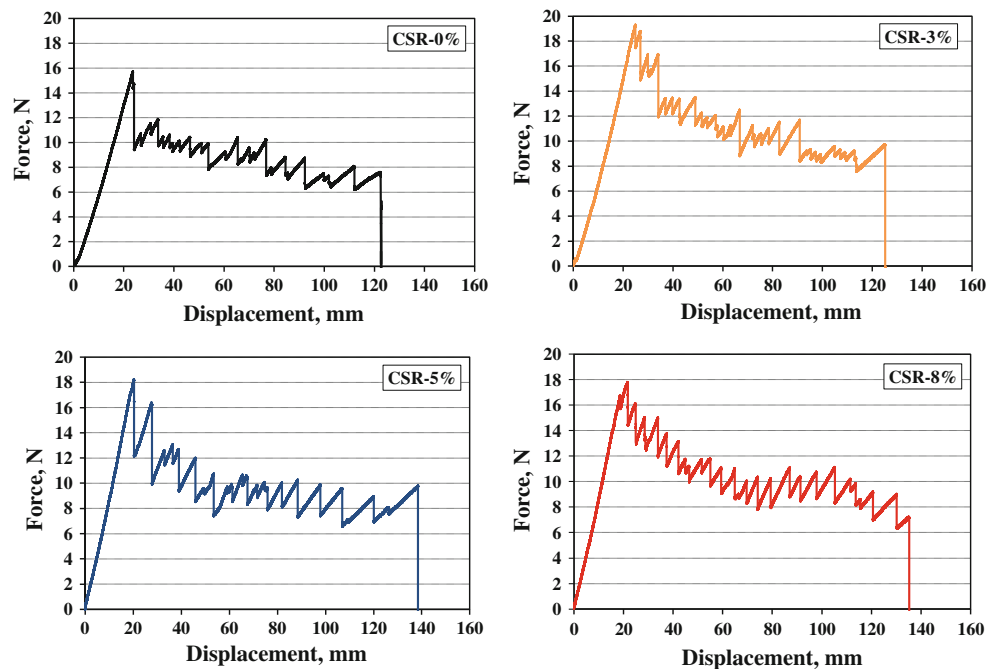


**Fig. 3** Typical delamination resistance (*R-curves*) of the CF/EP composites with various CSR contents

**Table 1** Initial and propagation delamination for the CF/EP composites with various CSR contents

CSR (wt%)	$G_{IC}$ (J/m <sup>2</sup> )	$G_{IP}$ (J/m <sup>2</sup> )
0.0	337.79 ± 15.50	398.08 ± 18.50
3.0	509.42 ± 16.50	573.15 ± 17.50
5.0	546.59 ± 17.50	595.58 ± 16.50
8.0	578.36 ± 14.50	630.84 ± 18.50

The mode I interlaminar initiation toughness ( $G_{IC}$ ) strongly depends on standard material property of composites, which related to a matrix-region ahead of the starter Teflon sheet. Therefore,  $G_{IC}$  value is mainly dominated by the matrix properties. As shown in Table 1, all the values of  $G_{IC}$  for the unmodified composite were lower

those for the modified composite. This reflected the enhanced fracture toughness of epoxy resin with the addition of CSR. Figure 3 showed that the fracture toughness values were nearly independent of crack length for all specimens. The similar results based on nanosized materials were found in which the fracture toughness values change considerably as the crack length increase [19, 21–23].

Moreover, it was found that initiation toughness values were lower than propagation toughness values. When the crack initiated to propagate, at that time, toughening mechanisms began to act. The increase of the energy was required for growing the crack further.

As shown in Fig. 3, the addition of CSR to the CF/EP composites strongly affected the initiation and propagation fracture toughness. It was clear that fracture delamination improved with the addition of various CSR contents. At 3.0 and 5.0 wt% CSR, the initial fracture toughness were increased by 50.80 and 61.81 %, respectively, and the propagation fracture toughness were increased by 43.97 and 49.61 %, respectively, in comparison with that of the unmodified CF/EP composite. A significant increase was observed for the initiation fracture toughness at 8.0 wt% CSR, the initiation fracture toughness was increased 71.21 % from 337.70 to 578.36 J/m<sup>2</sup>, the propagation fracture toughness was remarkably increased by 58.47 % from 398.08 to 630.84 J/m<sup>2</sup> which is a strong indicator of the reinforcing effect of CSR for improving interlaminar fracture toughness.

In general, a number of mechanisms show that the addition of the nanoparticles contribute to improvement of

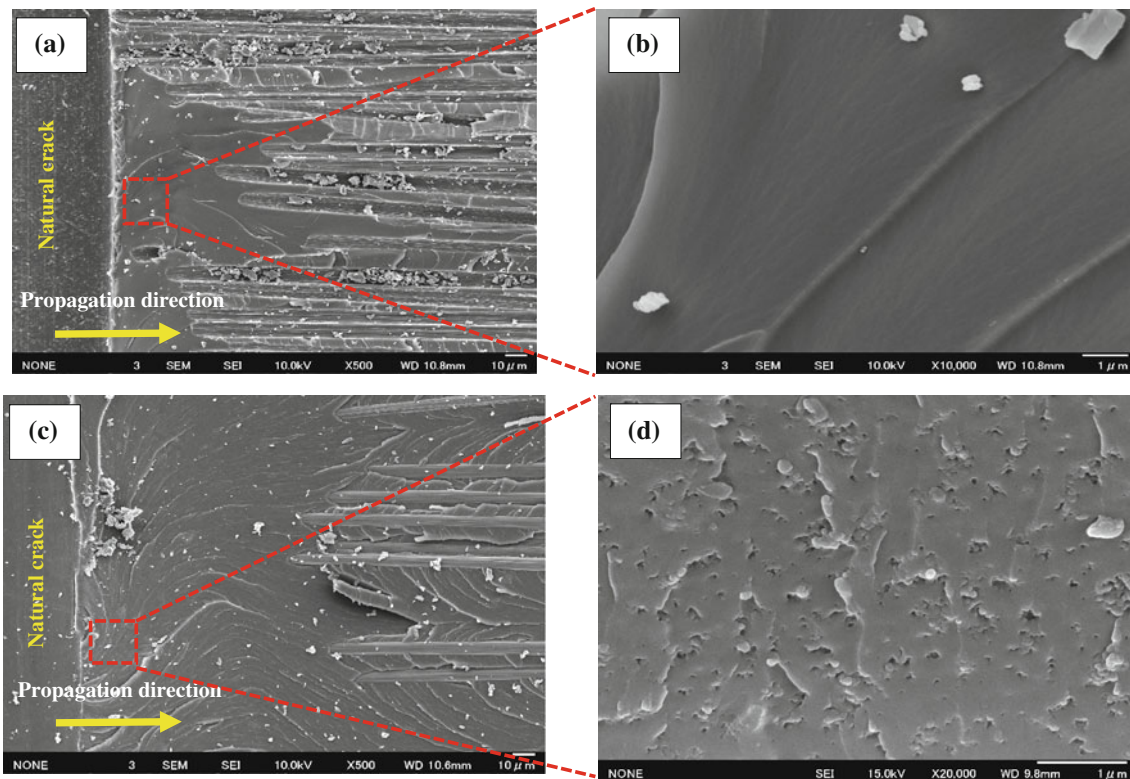


**Fig. 4** SEM images of the fracture surfaces for crack initiation: **a–b** the unmodified composite, **c–d** the modified composite

the fracture toughness, which is inclusion of rubber nanoparticles. It is often difficult to determine the dominant mechanism. Giannakopoulos et al. [24] stated that the operative toughening mechanisms of the nanoparticles in the epoxy polymer are the nanoparticle debonding, the shearing banding, and the plastic void growth. Hung-Jue Sue [25] showed that the nanoparticles induced the plastic void growth and the formation of the shear banding through extensive particle cavitation around a subcritically loaded crack tip. Hong-Yuan Liu et al. [26] reported the major toughness contributions for epoxy are the nanoparticle debonding, nanocavitation, and matrix plastic shearing. Jun Ma et al. [27] reported that the initiation and propagation of a thin dilatation zone and nanovoids as the dominant toughening mechanisms. Hui Zhang et al. [28] showed that the nanoparticles induced dimples and subdimples which cause energy dissipation. Johnsen et al. [14] stated that the nanoparticle debonding and the subsequent plastic void growth appeared to be the major toughening mechanism. Long-Chen Tang et al. [29] showed that a combination of rigid and soft nanoparticles induced the enlarged plastic deformation around the crack tip, which is a dominant factor in enhancing fracture toughness.

Scanning electron microscopy observation of the fracture surfaces of the specimens pronounced that there was a

distinct damage of interfacial region in the composite. For the unmodified composite, the fracture surfaces were mostly smooth and glassy due to brittle failure, as a result of the weak resistance to crack initiation and propagation. It also was seen that there are the formation of the pathways, microflow lines, and river patterns, which are characteristic of the brittle-like cracks along the macroscopic crack directions for both initiation and propagation fracture toughness (see Figs. 4a, b and 5a, b). Therefore, the required energy for the interlaminar delamination failure was low.

For the modified composite, as shown in Figs. 4c, d and 5c, d, the presence of CSR has a slight effect on the fracture surfaces at low magnification. It was found that the river marks in the matrix fracture areas appeared not to coincide with macroscopic crack growth directions, which suggested various directions of local microcrack growth. However, at higher magnification in Figs. 4 and 5 (at the right side), the modified CF/EP composite exhibited a rough fracture surface. It was found that numerous micro/nanovoids and microshear bandings were presented on the fracture surface. The formation of the observed patterns could be attributed to debonding of the rubber nanoparticles. The experiment results showed that the measured void size was slightly greater (about 40–45 nm) than the diameter of the rubber particles (about 35 nm) using



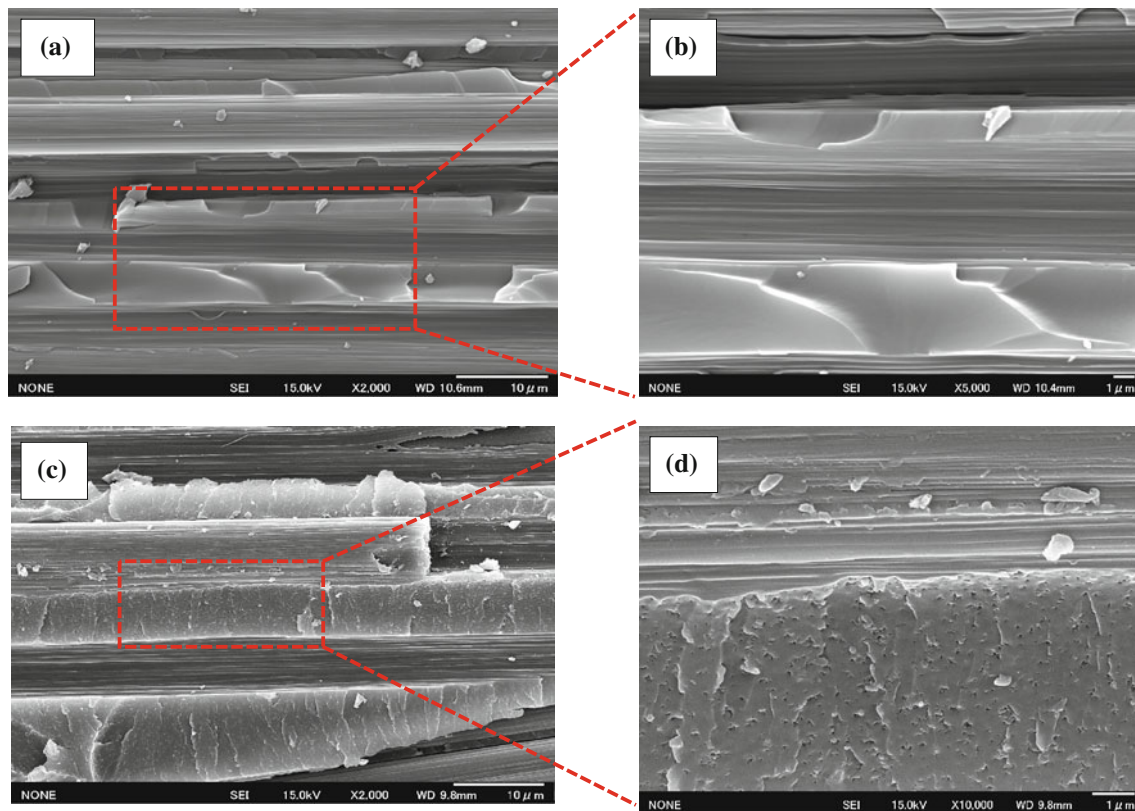


**Fig. 5** SEM images of the fracture surfaces for crack propagation: **a–b** the unmodified composite, and **c–d** the modified composite

EOS-7000F analysis software, indicating the plastic void growth occurred during crack propagation. It is worth mentioning that the formations of the rubber nanoparticle debonding, the consequent plastic void growth, and the microshear banding appeared as shown in Figs. 4d and 5d. These may lead to the creation of new fracture surface, and thus much fracture energy was likely dissipated. From the present results, it is safe to say that interlaminar fracture toughness of the CF/EP composites was increased by the addition of CSR. The rubber nanoparticle debonding, the plastic void growth, and the microshear banding are the dominate contributions for interlaminar fracture toughening effect of the CF/EP composites [30].

#### Tensile test

The effect of CSR contents on mechanical behavior of the CF/EP composites was investigated. Figure 6 showed that an increase of tensile strength for the modified composite. At 3.0 and 5.0 wt% CSR, tensile strength on the average was increased by 8.2 and 12.6 %, respectively. At 8.0 wt% CSR, tensile strength of the CF/EP composite was slightly increased by 9.25 %. This can be due to a undesirable agglomeration of the rubber nanoparticles at 8.0 wt% lead to a slight decrease trend in tensile strength in comparison with 5.0 wt% CSR. Manjunatha et al. [12]

reported that the addition of nanoparticles increased tensile strength of the neat epoxy and the GFRP by about 19.0 and 5.0 %, respectively. Uddin et al. [31] stated that tensile strength of the glass fiber/epoxy composite increased by about 11.0 % with the presence of the nanoparticles. It is pronounced that addition of nanoparticles played an important role in improving the strength of the interface. In this case, the nanosized fillers with large surface areas per unit gram led to the number of adhesively jointed points with carbon fibers was relatively high. As a result, an increase in tensile strength of the CF/EP composite was found. Young's modulus of the CF/EP composites, determined from the typical stress–strain curve, showed a little decrease at various CSR content ratios. This can be the fact that the modulus of carbon fibers is much higher than that of the epoxy matrix although the CSR contents in the CF/EP composites are relatively high up to 8.0 wt%. Other reason can be attributed to CSR is a solid nanoparticle (crosslinked rubber nanoparticles), leading to a rather hardness of rubber nanoparticle. It is totally different from liquid rubber such as carboxyl terminated butadiene nitrile (CTBN) in which a strong decrease of Young's modulus is found in composites [8, 22]. The slight decrease of Young's modulus also was revealed in epoxy system using CSR [12, 31].

**Table 2** Experimental results of fatigue test for the CF/EP composites with various CSR contents

Maximum cyclic stress (MPa)	Number of cycles to failure			
	CSR-0 (%)	CSR-3 (%)	CSR-5 (%)	CSR-8 (%)
600	5,200	356,044	436,744	324,679
600	5,730	421,226	495,632	358,079
600	4,459	466,324	526,343	437,567
570	19,879	1,887,780	2,487,780	1,689,093
570	21,345	1,946,378	2,746,378	1,890,579
570	24,599	2,190,482	2,904,821	1,987,651
530	134,135	>5,000,000	>5,000,000	>5,000,000
530	150,923	>5,000,000	>5,000,000	>5,000,000
530	167,020	>5,000,000	>5,000,000	>5,000,000

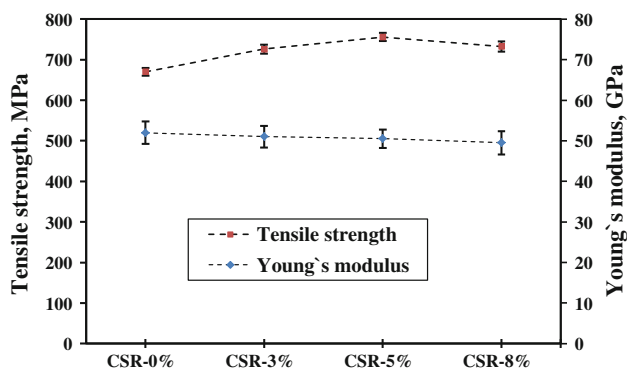


**Fig. 6** Tensile strength and Young’s modulus for the neat CF/EP composite and the modified CF/EP composites with various CSR contents

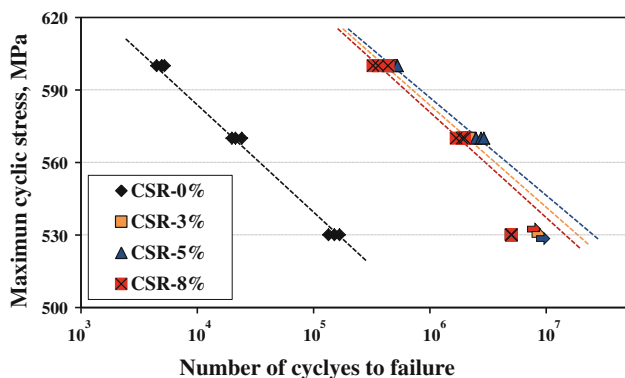
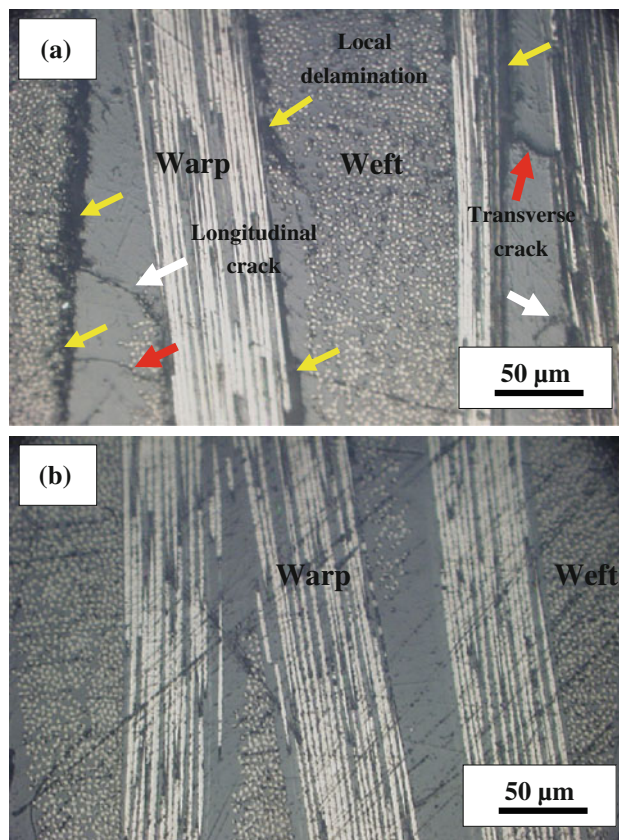


**Fig. 7** S–N diagrams of the CF/EP composites with various CSR contents

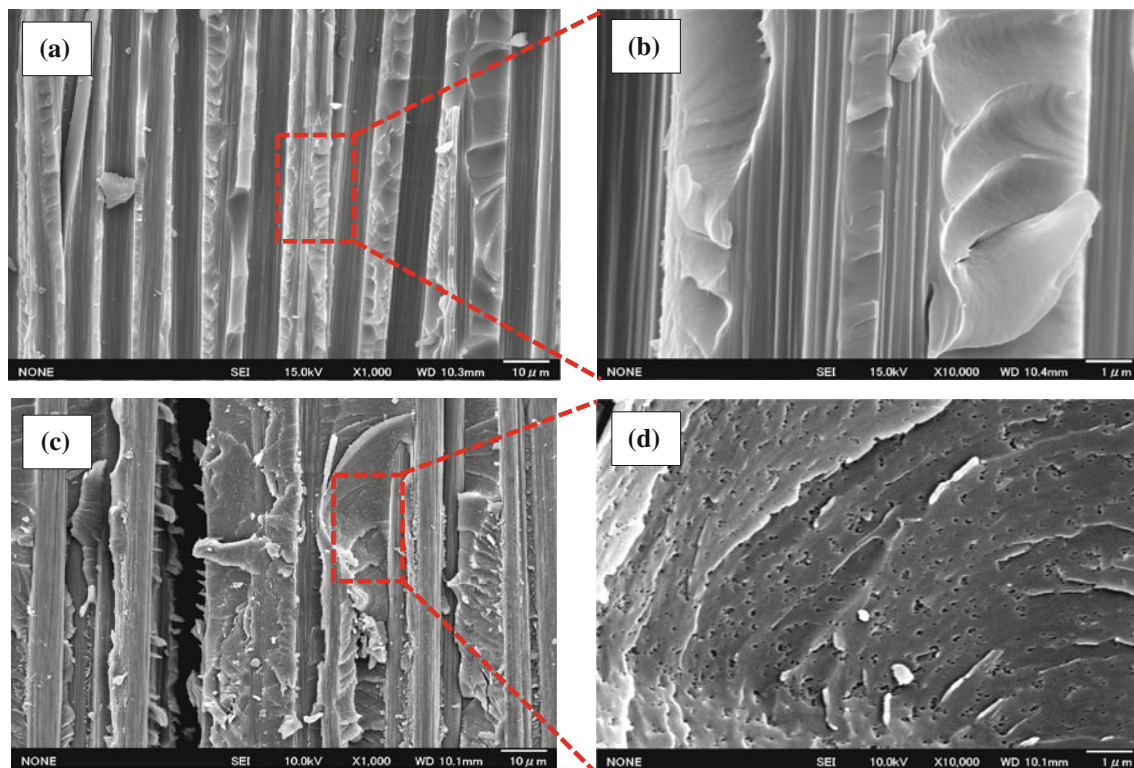
Tension–tension fatigue test

Table 2 listed the experimental results of fatigue test for the CF/EP composites with various CSR contents. Figure 7 showed the effect of CSR contents on the fatigue life by

depicting the stress–number of cycles to failure (S–N) curves. It revealed that fatigue life of the modified composite extended from 75 to 100 times than that of the unmodified composite at all maximum cyclic stress. At  $\sigma_{max} = 570$  MPa, it was worth noting that the durability of the CF/EP composites dramatically improved >100 times with the addition of 5.0 wt% CSR. A slightly decrease of fatigue life at 8.0 wt% CSR was observed. This can be due to an undesirable agglomeration of CSR occurred in the modified CF/EP composite. Furthermore, in Fig. 7, the slope of the S–N curves of the unmodified composite showed a strong drop, and lower than that of the modified composite at all maximum cyclic stress, which indicate the fatigue life of the unmodified composite was considerably sensitive to applied stress levels. The reason for the shift of the slope S–N could be attributed to the fact that the damage for the unmodified composite occurred earlier at all maximum cyclic stress [3, 12]. An observation of the internal damage at  $10^5$  cycles and the maximum cyclic stress of 530 MPa were performed using an optical microscopy at the side of the specimens. In Fig. 8a, the unmodified composite evidently revealed transverse cracks (indicated by red arrows), longitudinal cracks (indicated by white arrows), local delamination (indicated yellow



**Fig. 8** Microscopy images for the internal damage of the CF/EP composites: **a** the unmodified composite, **b** the modified composite



**Fig. 9** SEM images of the fracture surface of the CF/EP composites for the fatigue testing specimens: **a–b** the unmodified composite, and **c–d** the modified composite

arrows) along the warp, and the weft direction. On the other hand, the modified composite could not observe any cracks as shown in Fig. 8b.

The previous studies stated that various reasons caused the extension of fatigue life in the composites, such as the crack constrain using spread tows, the strength of transverse fibers bundles, the strength of longitudinal fiber bundles, the increases of quasi-static-fracture toughness, fiber bridging, particle bridging, particle debonding, fiber pull-out, the formation of smaller size dimples, the creation of nanoscale cracks, the plastic void growth, and the rubber cavitation [31–37]. However, it is often difficult to determine the dominant mechanism.

Field emission scanning electron microscopy observation of the fracture surfaces of the unmodified composite showed a brittle-like surface suggesting that the fatigue life was very sensitive under cyclic loading (see Fig. 9a, b). On the other hand, the fracture surfaces of the modified composites revealed the numerous nanovoids and the micro-shear bandings were presented at high magnification (see Fig. 9c, d). This can be believed due to toughening effects of CSR on the fracture surfaces for the modified composite, suggesting the fatigue life of which was insensitive under cyclic loading. Furthermore, it was found that the formation of new fracture surface resulted in a large number of nucleating sites for cracks to begin and grow. For a given

maximum cyclic stress, a large density of nanoscale cracks would grow more slowly than the lower density of larger microcracks present for the unmodified composite [34]. The obtained results were an increase in the number of cycles for initiation, propagation, and coalescence stage. This suggested that high-cycle fatigue life was enhanced with the presence of CSR. Based on aforementioned results, it is clearly credited that the rubber nanoparticles delayed the onset of matrix cracks, and reduce the crack growth rate through nanoparticle debonding and the plastic void growth mechanisms, which resulted in higher fatigue life in the CF/EP composites.

## Conclusions

In this study, we focused on our attention to improve the fracture toughness and fatigue life of the CF/EP composites by incorporating the CSR nanoparticles. The experimental results showed that the mode I interlaminar fracture toughness of the CF/EP composite containing 8.0 wt% CSR for both crack initiation and crack propagation significantly improved by 71.21 and 58.47 %, respectively. The fatigue life of the modified CF/EP composites dramatically increased 75–100 times longer than that of the unmodified composites at high cycle fatigue while the



tensile strength slightly increased by 10 %. FESEM observations of the fracture surfaces revealed that the rubber nanoparticle debonding followed by plastic void growth, plus microshear banding yielding, were the major mechanisms for delaying the onset of matrix crack, and reducing the crack growth rate of the CF/EP composites.

**Acknowledgements** The authors would like to thank Japan Synthetic Rubber Co, Ltd. for providing the core-shell rubber nanoparticles.

## References

- Khan SU, Kim J-K (2012) Carbon 50:5265
- Gkikas G, Barkoula N-M, Paipetis AS (2012) Compos B 43:2697
- Davis DC, Wikerson JW, Zhu J, Hadjiev VG (2011) Compos Sci Technol 71:1089
- Ashrafi B, Guan J, Mirjalili V et al (2011) Compos Sci Technol 71:1569
- Chen Q, Zhao Y, Zhou Z et al (2013) Compos B 44:1
- Zang G, Karger-Kocsis J, Zou J (2010) Carbon 48:4289
- Phong NT, Garb MH, Okubo K, Chuong B, Fujii T (2013) Journal of Materials and Design 47:624
- Phong NT, Garb MH, Okubo K, Chuong B, Fujii T (2013) Journal of Composite Structures 99:380
- Takagaki N, Okubo K, Fujii T (2008) Adv Mater Res 47–50:133
- Li G, Li P, Yu Y et al (2008) Mater Lett 62:511
- Hsieh TH, Kinloch AJ et al (2010) J Mater Sci 45:1193. doi: [10.1007/s10853-009-4064-9](https://doi.org/10.1007/s10853-009-4064-9)
- Manjunatha CM, Taylor AC, Kinloch AJ, Sprenger S (2012) Compos Sci Technol 70:193
- Boger L, Sumfleth J et al (2010) Compos A 41:1419
- Johnsen BB, Kinloch AJ (2007) Polymer 48:530
- ASTM 3039 (2008) Standard test method for tensile properties. American Society for Testing and Materials, West Conshohocken
- ASTM 5528–01 (2007) Standard test method for mode I inter-laminar fracture toughness. American Society for Testing and Materials, West Conshohocken
- ASTM 3479–96 (2007) Standard test method for tension–tension fatigue test. American Society for Testing and Materials, West Conshohocken
- Siddiqui NA, Woo RSC et al (2007) Compos A 38:449
- Zang G, Karger-Kocsis J, Zou J (2010) Carbon 48:4289
- Bortz DR, Merino C, Martin-Gullon I (2011) Compos Sci Technol 71:31
- Ashrafi B, Guen J et al (2011) Compos Sci Technol 71:1569
- Grabr MH, Elrahman MA, Okubo K, Fujii T (2010) J Mater Sci 45:3841. doi: [10.1007/s10853-010-4439-y](https://doi.org/10.1007/s10853-010-4439-y)
- Imanaka M, Motohashi S et al (2009) Int J Adhes Adhes 29:45
- Giannakopoulos G, Masania K, Taylor AC (2011) J Mater Sci 46:327. doi: [10.1007/s10853-010-4816-6](https://doi.org/10.1007/s10853-010-4816-6)
- Sue H-J (1991) Polymer Eng Sci 31(4):270
- Liu H-Y, Wang G-T, Mai Y-W, Zeng Y (2011) Compos B 42:2170
- Ma J, Mo M-S, Du X-S (2008) Polymer 49:3510
- Zhang H, Zhang Z, Friedrich K, Eger C (2006) Acta Materialia 54:1833
- Tang L-C, Zhang H (2012) Compos Sci Technol 7:558
- Huang Y, Kinloch AJ (1992) J Mater Sci 27:2763. doi: [10.1007/BF00540703](https://doi.org/10.1007/BF00540703)
- Uddin MF, Sun CT (2008) Compos Sci Technol 68:1637
- Liu H-Y, Wang G, Mai Y-W (2012) Compos Sci Technol 72:1530
- Bortz DR, Merino CM, Martin-Gullon I (2011) Compos Sci Technol 71:31
- Grimmer CS, Dharan CKH (2008) J Mater Sci 43:4487. doi: [10.1007/s10853-008-2651-9](https://doi.org/10.1007/s10853-008-2651-9)
- Nishikawa Y, Okubo K, Fujii T (2006) Int J Fatigue 28(10):1248
- Boger L, Sumfleth J, Hedemann H, Schulte K (2010) Compos A 41:1419
- Jen Y-M, Wang Y-C (2012) Compos B 43:1687